Bulletin of Electrical Engineering and Informatics
Vol. 14, No. 6, December 2025, pp. 4356~4367
ISSN: 2302-9285, DOI: 10.11591/eei.v14i6.10455

Modeling broken rotor bar faults in induction motors: a combined SSFR and FEM approach

Abdelhakim Mabrek[1], Zaidi Elyazid[2], Bachir Selmoune[2], Kamel Eddine Hemsas[3]
[1]Intelligent Materials and Renewable Energy Laboratory LMIER, Department of Electromechanics, Faculty of Science and Technology, EL Bachir El Ibrahimi University, Bordj Bou Arreridj, Algeria
[2]Department of Electromechanics, Faculty of Science and Technology, EL Bachir El Ibrahimi University, Bordj Bou Arreridj, Algeria
[3]Setif Automatic Laboratory LAS, Department of Electrical Engineering, Faculty of Technology, University Ferhat Abbas, Setif, Algeria

Article Info

Article history:

Received Apr 11, 2025
Revised Sep 14, 2025
Accepted Sep 27, 2025

Keywords:

Broken bar
diagnostic
Finite element
Frequency response
Harmonics analyses
Standstill

ABSTRACT

The fault of broken rotor bar (BRB) yields to high levels of stress in induction motor drive (IM) and being a common fault. This paper proposes a novel hybrid approach combining standstill frequency response (SSFR) testing and finite element method (FEM) modeling to improve fault diagnosis accuracy. The findings were verified experimentally using a 7.5 kW three-phase IM by SSFR approach under various failure scenarios. Reliability of SSFR method is confirmed by the use of FEM, flux 2D magnetic analysis software is employed on the same IM using in SSFR to determine the magnetic field under different fault and load conditions. The work is finished by current harmonics analyses and the outcomes of the BRB model demonstrate that the combined method enhances fault detectability, particularly for incipient and partial bar breakages, reducing false alarms compared to conventional techniques.

Corresponding Author:

Abdelhakim Mabrek
Intelligent Materials and Renewable Energy Laboratory LMIER, Department of Electromechanics
Faculty of Science and Technology, EL Bachir El Ibrahimi University
34030 El-Anasser, Bordj Bou Arreridj, Algeria
Email: abdelhakim.mabrek_1@univ-bba.dz

1. INTRODUCTION

Due to their critical importance in diverse industriel aplications, the induction motor drive (IM) is the most common electrical machine [1]. Open circuit, bearing failures, short circuit faults, and BRB faults are common categories for the problems in the IM. According to [2], the broken rotor bar (BRB) is a serious failure that might lead to to stoped production and result in significant financial loss. Fault modeling is crucial for improving IM fault detection methods because it provides a detailed understanding of how different faults affect the motor's electrical and mechanical behavior. It was the first phase of building fault detection systems. These models enable precise assessment by simulating both transient and steady-state motor behaviour [3].

A wide variety of modeling techniques have been developed over time. Numerous studies have been conducted in recent years, and several academics have become interested in modeling the BRB defects in IMs. Mustafa *et al*. [4] suggest an approach for evaluating the sanity of motors in the event that both healthy and defective data are not available. They use a model-based support vector classification (SVC) technique that uses features derived from the spectrum analysis of the stator's steady state current to detect broken bars in IM under full load situations. A precise mathematical model for the IM that can incorporate BRB faults with varying severities is proposed in paper [5]. To create such an analytical model, multiple coupled circuit modeling is used, in [6] the time-stepping finite element (TSFE) analysis is one of the most used techniques

for modeling IMs with defective rotor bars, a comparison of the healthy and faulty cases is done. To explain the parametric change of a defective IM model, an easy-to-understand model in an ABC frame is presented [7]. A unique fault model has been created to identify parameters by looking at specific parts of the transfer functions of the IM using certain model structures [8]. To take into account both healthy and broken bar circumstances, researchers in [9] propose a transient model of IM that relies on self and mutual inductance estimates based on finite element analysis (FEA). The work in [10] examines the BRB for the IM, investigates local saturation to see how the machine operates, and includes the nonlinear B-H curve and magnetic-equivalent-circuit (MEC) to clarify the saturation effect and the machine model. An IM with BRB is modeled using the time stepping finite element method (TSFEM), all of the motor's geometrical and physical properties are included in this modeling [11], [12].

Numerous academics employ standstill testing to detect rotor anomalies in IMs. The authors of [13], [14] investigate the potential use of the stationary impedance variation test in the identification of the BRB defect in inverter-fed IMs. The researchers [15], [16] examine the feasibility of detecting the rotor faults of induction machines by performing standstill tests, it is possible to excite with low-frequency resolution the faulty modes. Machine learning-based models (ML) have shown significant promise in accurately predicting the failure of broken bar IMs. Various approaches leverage advanced algorithms and large datasets to enhance diagnostic accuracy. Tahkola *et al.* [17] demonstrates that ML-based models can accurately predict BRB failures in IMs using simulated and measured data, achieving similar accuracy with both logistic regression and cat-boost classifiers, particularly with raw fast Fourier-transformed signals. The proposed AI-based approach in the paper demonstrates a highly effective detection and classification of BRB in IMs, achieving 98% accuracy and a prediction time of 1.64 microseconds, indicating strong potential for accurate failure prediction [18]. Table 1 give a comparative summarizing key methods with metrics.

Table 1. Modeling BRB methods comparison

Method	Fault sensitivity	Computational cost	Key limitations
TSFEM	Very high – Directly models – Fault location	Extremely high – Requires significant resources and time	– Prohibitive computational cost, requires expert knowledge
MEC	High – Model fault more accurately than analytical models	Medium – Much faster than TSFEM, but slower than analytical models	– Model complexity increases with accuracy – Reluctance network must be well designed
SVC	High (for diagnosis) – Excellent at separating classes when trained properly	Low (inference) – Classification is very fast – Requires large, labeled datasets	– Requires extensive, labeled, real world data for training – "Black box" model with no physical insight
ML based models	Very high – Can detect subtle, complex patterns missed by traditional methods	Very high (training) – Requires massive data and GPU resources – Medium (inference)	– Highest data requirements – Most “black box” approach – Performance is opaque and hard to trust without explanation

Due to limitations of existing detection techniques, a novel approach involves using the standstill frequency response (SSFR) test to extract a high-fidelity set of motor parameters under a fault condition. The novelty is validating the accuracy of these extracted parameters by comparing them against the internal magnetic flux distribution obtained from a FEM simulation of the same faulty motor. This bridges the gap between easy-to-measure electrical tests and the ground-truth physical reality inside the motor (FEM flux maps). It proves that the SSFR-derived parameters are physically meaningful and sensitive to the fault. This has not been done comprehensively before and would be a significant contribution. In this paper a new technique for BRB fault modeling is developed using the SSFR and FEM as an intelligent scheme. The various faults EC identification has been studied in order to increase accuracy and reduce diagnosis error rate.

2. METHOD

The specific advantage of combined SSFR-FEM method is that it provides a safe, low-cost, and repeatable pathway to empirical truth in a field often dominated by simulation and indirect measurement. This is a highly valuable contribution, like show Figure 1, the proposed method can be summarized in for steps:

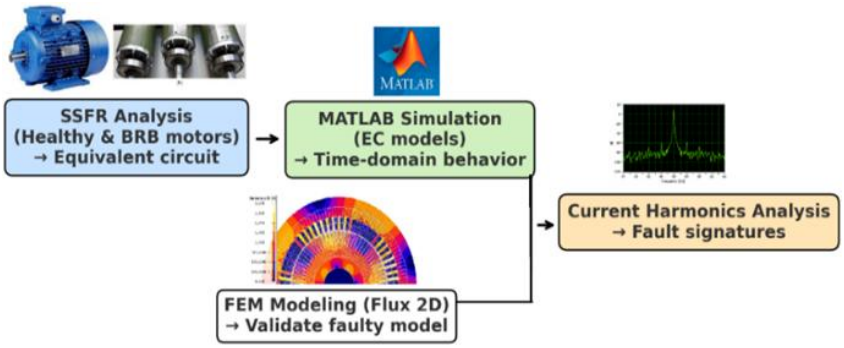

Figure 1. Diagram of the SSFR-FEM workflow

2.1. Standstill frequency response-finite element method workflow

SSFR analysis of the healthy and faulty IM: to perform equivalent circuit at standstill:

a. Prepare motor and safety: lock rotor and ensure thermal limits won't be exceeded during low-voltage.
b. Induce BRBs in controlled manner and record exact location and number.
c. Inject low-amplitude AC voltage at stator terminals sweeping logarithmically from ~0.1 Hz to ~1 kHz.
d. Measure terminal currents and voltages using averaging and windowing to reduce noise.
e. Compute transfer function (Vs/Is) to extract magnitude and phase and obtain frequency response.

Building MATLAB simulation using the EC model:

a. Fit an EC (choose multi-branch rotor structure to capture deep-bar effects) to the SSFR data using nonlinear least squares (Levenberg–Marquardt) to obtain EC model.
b. Implement SSFR-derived EC in time-domain Simulink. Run scenarios of healthy/faulty IM.
c. Modeling IM with BRB using the FEM:
d. Build a 2D FEM model (airgap, stator/rotor slots, bar conductors).
e. Represent broken bars by setting conductivity to near zero or by introducing an insulation gap.

Current harmonics analyses:

a. Implement SSFR-derived EC in time-domain Simulink. Run scenarios of fault/no-fault and compare current harmonics and torque pulsations with FEM outputs.
b. Ratios of spectral lines (sidebands around supply harmonics), specific frequency peaks.

2.2. Standstill frequency response

The IEEE committee suggested the SSFR method in 1983, and the studies that serve as its theoretical foundation [19]. In order to carry out these tests, the machine is powered only by two phases of the stator with a variable amplitude and variable frequency sinusoidal voltage source V_s, when the rotor speed is null, the operational impedance Z_s of the IM can be measured from stator terminal. In order to measure these impedances, a frequency signal is supplied to a single winding, and the amplitude and phase of the input current *Is* are recorded as the frequency is changed. Once these measurements are obtained, the machine's parameters may be established [20], [21].

Tests are performed on a bench (Figure 2), which contains; (a) frequency generator (0.1 Hz to 1000 Hz) with fixed voltage, (b) 2 pole IM, 7.5 kW, 400/230V with broken cage bar, (c) personal computer with software CASSY_LAB, and (d) sensor card Cassy_Lab.

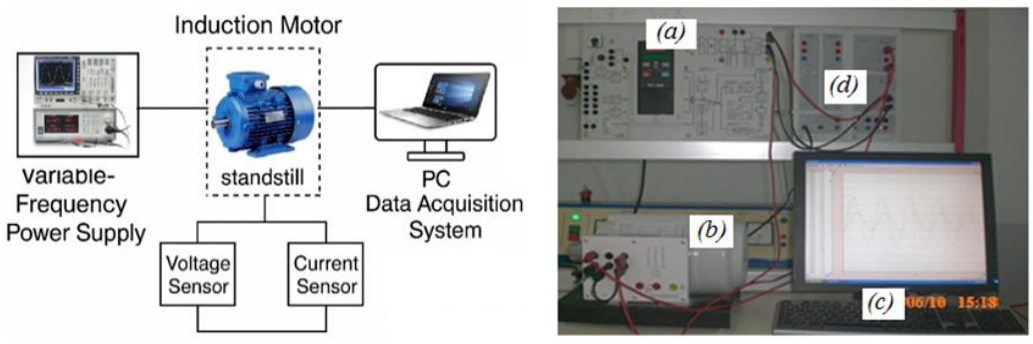

Figure 2. Experimental unit of IM with broken bar at standstill

A series of SSFR measurements are made on the three motors at standstill and with a reduced voltage (10 V) and variable frequency ranging from ω=2πf=0.1005 Hz to 995.88 Hz. The frequency analyzer records the vectors, frequency, amplitude and phase shift between the current and the voltage. Then we can determine: magnitude (dB) response vs. frequency in Figure 3. The SSFR test allows for the derivation of the motor's operational inductance $L_d(p)$ and $L_q(p)$ (the direct and quadrature axis inductances) as functions of the Laplace variable p (or frequency).

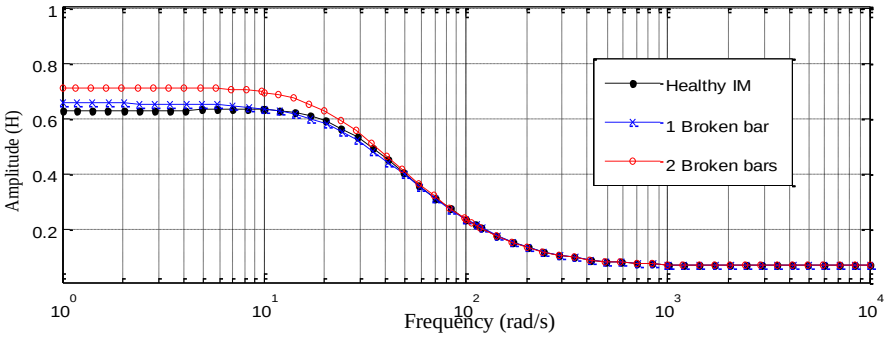

Figure 3. Experimental inductance variation versus BRB

A BRB creates an asymmetry in the rotor cage, which breaks the magnetic symmetry of the rotor. This asymmetry is directly captured by a growing discrepancy between Ld(s) and Lq(s), a condition known as saliency, which is not present in a healthy squirrel-cage motor. Table 2 quantifies how the key operational inductance parameters change with the severity of the BRB.

Table 2. Comparison of operational inductance variation as a fault indicator

Parameter/indicator	Healthy motor (symmetric rotor)	Motor with BRB(s)	Quantified change and physical explanation
Direct axis operational inductance, Ld(s)	For a symmetric rotor, Ld(s)≈Lq(s) across all frequencies. The curves are nearly identical.	Decreases slightly. The path for d-axis flux is marginally affected as the fault introduces asymmetry and increases leakage.	-2% to -8% in the mid-frequency range. The effective impedance to the d-axis flux increases slightly due to the distorted rotor current path.
Quadrature axis operational inductance, Lq(s)	Lq(s)≈Ld(s) across all frequencies.	Decreases more significantly than Ld(s). The q-axis flux path is more severely disrupted by the broken bar.	-5% to -15% in the mid-frequency range. BRB creates a significant barrier for q-axis currents, increasing leakage and reducing the effective inductance.
Saliency (Ld(s) vs Lq(s))	No saliency. Ld(s)/Lq(s)≈1 across the entire frequency spectrum. The rotor appears isotropic.	Emergence of saliency. A clear and measurable difference appears, where Ld(s) > Lq(s). This is a primary fault signature.	The ratio Ld(s)/Lq(s) becomes > 1. A ratio of 1.03 to 1.20+ is observable, increasing with fault severity. This quantifies the induced asymmetry.

2.3. EC model identification

The goal is to find the parameters of the IM's equivalent circuit presented in Figure 4, (e.g., stator resistance Rs, stator leakage inductance Lσs, rotor resistance Rr1-Rr2, rotor leakage inductance Lσr1-Lσr2, magnetizing inductance Lm) that make OE model's predicted impedance best match the measured impedance across all frequencies, with ψs, and ψr are the stator and rotor flux in the d axis.

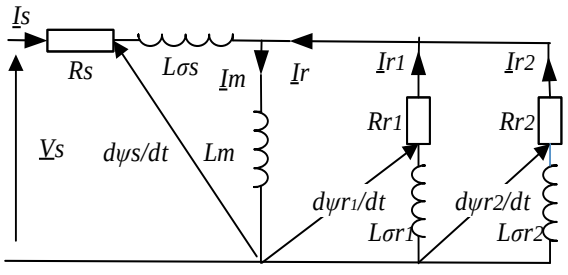

Figure 4. The D-axis EC model parameters at standstill

The OE estimation algorithm is used to identify the transfer function model parameters, the transfer function from *"*frequency input*"* to *"*impedance output*"*. The stator impedance is a complex function of the Laplace variable *p*.

$$Z_s(p) = \frac{V_s(p)}{I_s(p)} = R_s + pL_{\sigma s} + \frac{1}{\frac{1}{pLm} + \frac{1}{Rr1+pL\sigma r1} + \frac{1}{Rr2+pL\sigma r2}} \quad (1)$$

This can be rewritten as a ratio of polynomials:

$$Z_s(p) = \frac{b_0p^4+b_1p^3+b_2p^2+b_3p+b_4}{a_0p^4+a_1p^3+a_2p^2+a_3p} \quad (2)$$

The coefficients b0, b1,.., b4, a0, a1, a2, a2 are nonlinear algebraic functions of the 7 physical parameters we want to find, then fitting a discrete-time model that approximates the continuous-time impedance.

OE model structure should be: OE (nb, nf, and nk), nb=5 (number of numerator coefficients, b0 to b4), nf=4 (number of denominator coefficients, f1 to f4, since f0=1, f0=1), nk=0. The identifyied model is given by (3), where q is the shift operator, and the input is "frequency":

$$\hat{Z}(q,\theta) = \frac{B(q)}{F(q)} = \frac{b_0q^{-0}+b_1q^{-1}+b_2q^{-2}+b_3q^{-3}+b_4q^{-4}}{1+f_1q^{-1}+f_2q^{-2}+f_3q^{-3}+f_4q^{-4}} \quad (3)$$

The goal is to find the OE coefficients θ that minimize the sum of squared errors between the measured Z and the model's prediction $\hat{Z}$ using the gauss-newton loop:

$$\theta = [b0, b1, b2, b3, b4, f1, f2, f3, f4] \quad (4)$$

Once we have the optimal OE coefficients θ, we must solve the system of nonlinear equations to find the physical motor parameters *[Rs, Lσs, Lm, Rr1, Lσr1, Rr2,* and *Lσr2].* This is itself another nonlinear least-squares problem, we can use the Levenberg-Marquardt algorithm here. An EC have two rotor circuits is give in Table 3.

Table 3. The equivalent circuit parameters of IM

Parameter	Healthy motor	1 broken bar	2 broken bars	Δ (1BB) %	Δ (2BB) %
Rs (Ω)	1.70	1.70	1.70	+0.0	0.0
Lσs (mH)	30	30.1	3.0	0.0	0.0
Lm (mH)	190	177	165	-0.68	-1.35
Rr1 (Ω)	1. 9	2.6	3.2	+36.84	+68.42
Lσr1 (mH)	1	1. 1	1.3	+10	+30
Rr2 (Ω)	3.70	4.05	5.03	+9.4	+35.94
Lσr2 (mH)	3.2	4.0	5.2	+22	+62.5
FPE	0.0114	0.0112	0.0040	x	x

The identification technique used is the output error (OE) method, and the search direction to minimize the criteria can be calculated using the Gauss-Newton method for minimizing the final prediction error (FPE).

$$FPE=LF*(1+2*d/M) \quad (5)$$

Where LF is the loss function, d is the number of estimated parameters, and M is the number of estimation data samples, denoted as d<<M. The machine model is estimated using the IDFRD routine from the experimentally delivered frequency response.

- The dramatic increase in Rr1 and Rr2 is the clearest signature of the broken bar fault. The severity of the fault (1 BRB vs 2 BRB) is clearly reflected in the magnitude of the increase.
- The fact that Rs, Lσs, and Lm remain relatively constant confirms that the changes in rotor parameters are not due to measurement error or temperature drift but are indeed caused by the rotor fault.
- The changes in leakage inductances Lσr1 and Lσr2 provide supporting evidence for the fault.

2.4. Modelling broken rotor bar based on finite element method analysis

In this section, a squirrel cage IM is simulated using FLUX-2D software, and its performance under BRB faults is examined. A robust FEM study for this purpose requires careful configuration [22], [23].

a. Boundary conditions:
1) Periodicity: use Master-Slave boundary conditions on the radial boundaries of a pole-pair segment to simulate the full machine.
2) Excitation: for the stator windings, applied a three-phase, sinusoidal current source excitation. The current amplitude should be set based on the motor's rated current (e.g., for a 7.5 kW, 400 V motor, ~15 A line current, 2880 rpm nominal speed, tow pole). In rotor bars, for a transient analysis, the rotor circuit can be short-circuited by connecting the end rings.
3) Motion setup: for transient analysis with motion, define a band region around the rotor and specify rotational motion with an initial mechanical load.

b. Mesh density and strategy:

A poor mesh will render all results invalid and structured strategy is essential.
1) Strategy: curvature-based meshing with a minimum number of elements per circle (e.g., 12-18).
2) Critical regions for refinement: air gap requires the finest mesh due to the rapid decay of fields. At least 3-5 elements across the radial length of the air gap, stator/rotor tooth tips (highly saturated regions with complex flux paths). Conductors skin effect must be captured, especially at higher frequencies. Around BRB the flux distortion is localized; a finer mesh here captures the anomaly accurately.

c. Convergence study, the process is:
1) Solve the model with a coarse mesh.
2) Refine the mesh globally (e.g., reduce element size by 25%) and solve again.
3) Compare a key result (e.g., torque ripple, stator current) between the two solutions.
4) Repeat steps 2-4 until the change in the result is below a predefined threshold (e.g., <1-2%). The mesh before the final refinement is considered “converged”.

d. Solver type and setup:
1) Type: transient/motion with time-stepping. This is mandatory to capture fault harmonics, torque ripple, and speed oscillations caused by broken bars. Magnetostatic solvers are useless for this fault.
2) Time step: critical for accuracy and stability. Must be small enough to resolve the fastest dynamics.
3) Rule of thumb: time Step < 1/(20*f_max), where f_max is the highest frequency of interest. For broken bar analysis, sidebands around the fundamental (50/60 Hz) are key, so f_max is ~150-200 Hz. A time step of 0.1 to 0.5 ms is usually appropriate.
4) Duration: simulate enough electrical cycles to reach steady-state (5-10 cycles) and then several more cycles to capture the low-frequency oscillation caused by the fault (1-2 seconds total simulation time). Meshing of study domain and problem solving is given in Figure 5.

FLUX-2D was used to create IM model, three scenarios were analyzed to investigate the BRB fault: a healthy rotor, one broken bar, and two broken bars. This fault was simulated by removing the designated number of bars, as depicted in Figure 6(a) the currents in the bars produce a symmetrical distribution of flux lines around each pole, in contrast, the broken bars do not conduct current Figure 6(b), indicating any localized demagnetization effect in the broken bar region. This results in a magnetic flux concentration and an asymmetrical distribution surrounding the damaged bar. Furthermore, an increase in BRB exacerbates the disparity in the flux line distribution Figure 6(c). Which can be used to diagnose defects by monitoring changes in magnetic flux [24].

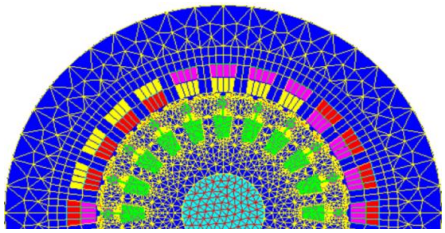

Figure 5. Complete geometrical 2D model of the IM

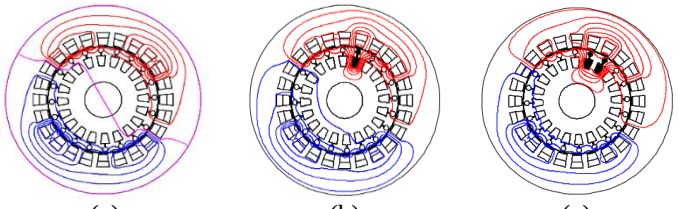

(a) (b) (c)

Figure 6. Different cases of faults; (a) healthy, (b) one BRB, and (c) two BRB

3. RESULTS AND DISCUSSION

3.1. Simulation based on standstill frequency response and finite element method

With the comprehensive model of the IM established, it is now pertinent to analyze the evolution of temporal quantities such as currents, torque, and speed in the event of rotor failure, utilizing electromagnetic characteristics and the FEM model. During the initial phase of IM operation, specifically within 0 to 0.5

seconds, there is no indication of rotor failure. This period is characterized by current amplitudes peaking at approximately 60 A, as illustrated in Figure 7(a). Following this phase, a steady state is achieved, resulting in a decline in current to exhibit sinusoidal oscillations around 5 A. When a nominal resistive torque of 25 Nm is applied, the current levels rise, potentially exceeding a maximum of 20 A, as depicted in Figure 7(b).

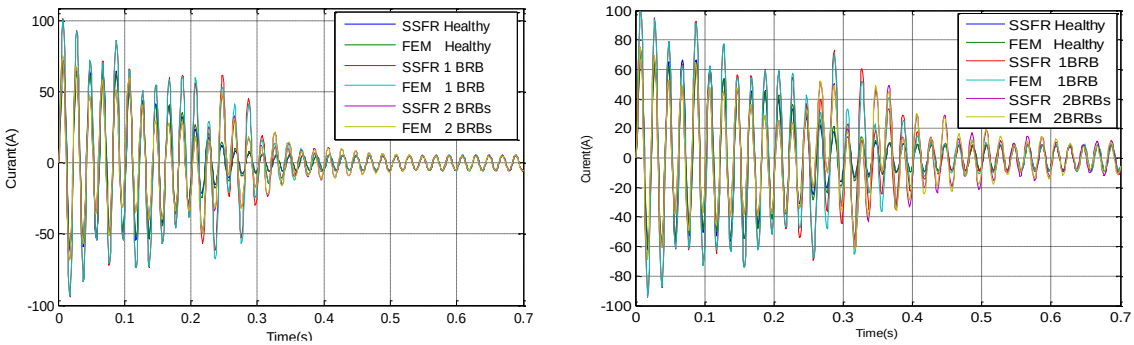

(a) (b)

Figure 7. Stator current of the healthy and faulty rotor; (a) no load and (b) full load

Rotor bar failures induce current imbalances, with amplitude increasing proportionally to the number of broken bars. Notably, the amplitude of the oscillations also depends on the load, which contributes to accelerated aging of the motor components, thereby elucidating the cumulative effect that results in the fracture of the bars. Figure 8(a) presents the simulation outcomes of the electromagnetic torque under no load conditions for scenarios involving 0, 1, and 2 broken bars. The ripple content within the torque escalates as the severity of the fault intensifies. These ripples become even more pronounced when subjected to full load conditions, as Figure 8(b) illustrates. Notably, as rotor resistance increases, the rotor current diminishes, reducing the opposing armature reaction. This reduction results in an enhancement of the net flux within the air gap. Given the direct proportional relationship, a more substantial flux yields an increase in torque.

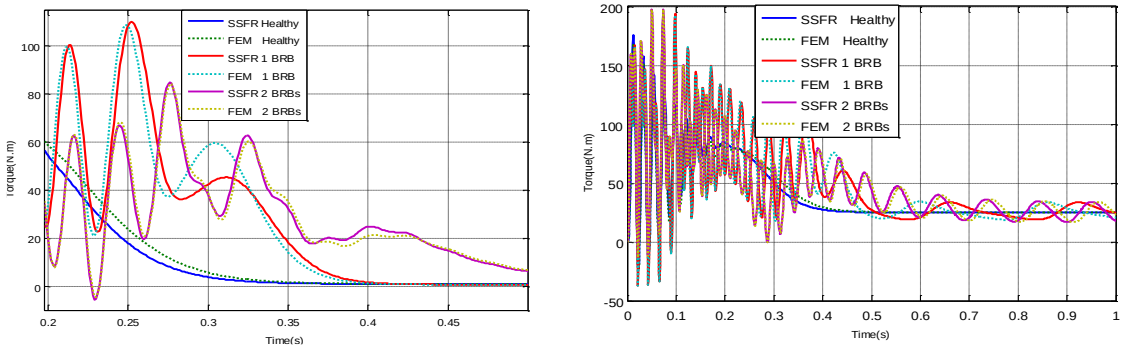

(a) (b)

Figure 8. Torque of the healthy and faulty rotor; (a) no load and (b) full load

Figure 9(a) depicts the evolution of speed during startup. Initially, the speed rises from 0 to 3000 rad/s within 0.5 seconds, reaching a steady state. However, introducing a resistive torque of 25 Nm slows down the motor shaft, resulting in a decrease in speed Figure 9(b) illustrates how the presence of BRBs influences the duration of the transient regime during startup. These broken bars affect the transient operation time. A comparison between a machine in good condition and one with faults reveals that startup time increases with the number of broken bars.

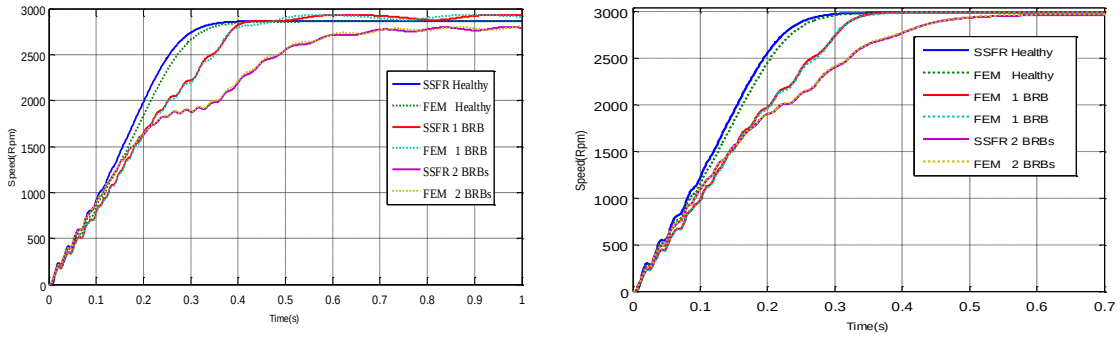

Figure 9. Speed of the healthy and faulty rotor; (a) no load and (b) full load

3.2. Study of healthy and broken rotor bar motors current harmonics

The BRB model obtained from the SSFR test is validated by means of motor current signature analysis (MCSA). The study's 500 Hz bandwidth restriction allows for a focused analysis of low-frequency phenomena and guarantees that the frequency-domain induction machine model is limited to pertinent factors like sources of current, voltage, resistances, and inductances [25], [26].

$$Fb = Fn(1 \pm 2ks),\ k = 1,2,3, \quad (6)$$

The fault frequency component is observed near the fundamental frequency of 50 Hz. When the system is at no load, the fault frequencies are not detectable because they are very close to the fundamental frequency (Fn). Under load conditions, the slip is calculated to be 4%. As a result, the faults generate higher and lower frequency components. Using in (6), we find that Fb1 is 46 Hz and Fb2 is 54 Hz [27].

a. No BRB fault: the healthy IM is first simulated under no-load. Figure 10(a) illustrates the stator current spectrum at the motor's rated speed, with a fundamental amplitude recorded at 7.5 dB (50 Hz). Under a load of 25 Nm resistive torque “Figure 10(b)”, the value is recorded at 12.5 dB (50 Hz). It is essential to observe that the current spectrum does not display any harmonics.
b. One BRB fault: Figure 11(a) depicts the power spectrum of the defective IM exhibiting a single broken BRB under no load conditions. The fault frequencies are 46 Hz and 54 Hz, corresponding maxima of -75.83 dB and -73.3 dB, respectively. At maximum load “Figure 11(b)”, fault frequencies are detected at 46 and 54 Hz, corresponding peaks of -70.92 dB and -72.64 dB, respectively. The results demonstrate that the amplitude of the fault frequency escalates with an increase in load.
c. Two BRB fault: the fault's severity has intensified, with power spectrums for no-load and full-load circumstances depicted in Figures 12(a) and (b), respectively. This defect produces supplementary harmonic line current components at no load (46 Hz, -69.46 dB and 54 Hz, -72.00 dB), and full load (46 Hz, -60.13 dB and 54 Hz, -59.41 dB). The results indicate that fault frequencies escalate with load and severity.

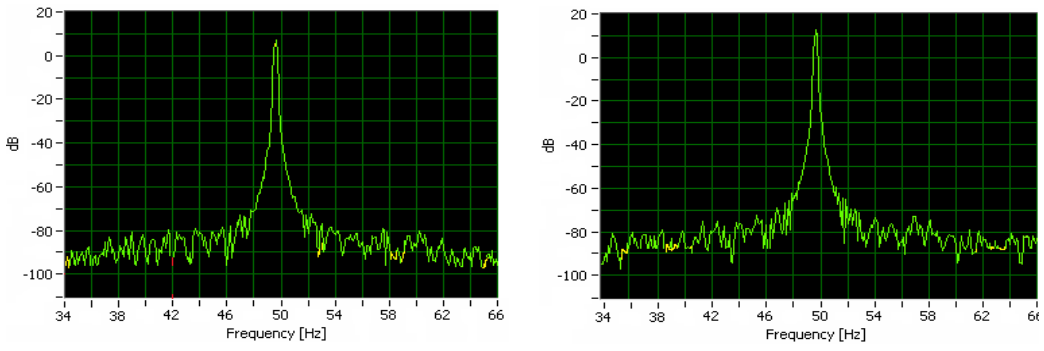

Figure 10. Current spectrum density for healthy motor; (a) under no load and (b) under load

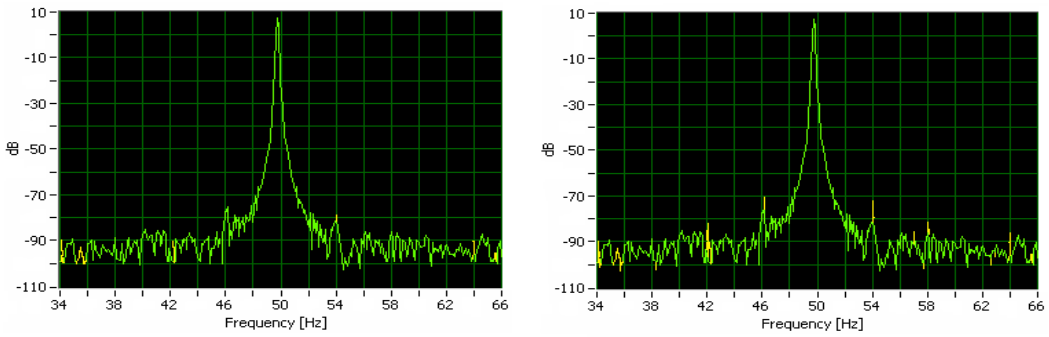

Figure 11. Current spectrum density for 1 broken bar; (a) under no load and (b) under load

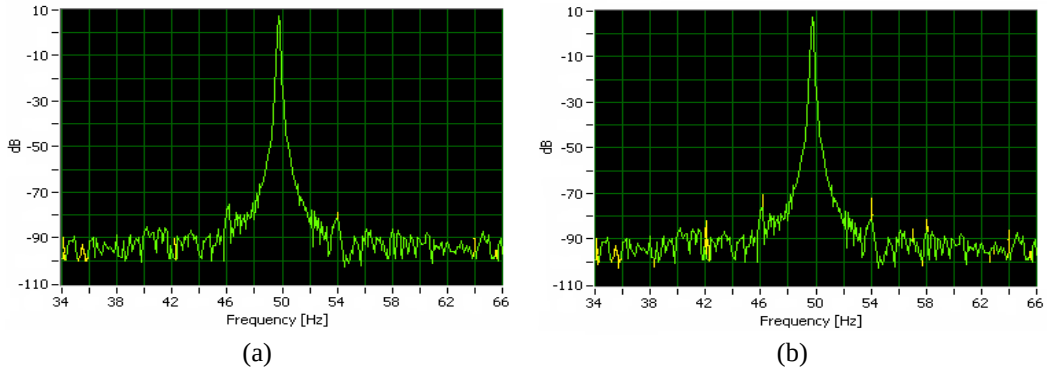

Figure 12. Current spectrum density for 2 broken bars; (a) under no load and (b) under load

3.3. Discussion and interpretation

While not suited for online monitoring, SSFR is an invaluable tool for confirming faults suspected by MCSA, for precise model-based simulation of faulty motors. The results of the simulations and experiments allowed us to conduct the following discussion and interpretation:

a. Current analysis: BRBs induce an imbalance in the current waveforms. The severity of this imbalance is proportional to the number of broken bars and is exacerbated by higher loads, leading to accelerated wear and further bar fractures.
b. Torque analysis: broken bars increase effective rotor resistance. This reduces rotor current and its opposing magnetic field, leading to a stronger net magnetic flux in the air gap. Since torque is directly proportional to flux, this results in a torque increase in the faulty sections, creating the observed ripple.
c. Speed analysis: the motor accelerates from 0 to 3000 rad/s in 0.5 s, broken bars negatively impact performance during the transient startup period. The time required to reach operating speed increases with the number of broken bars, indicating a loss of efficiency and available torque.
d. Spectral analysis: the simulation successfully demonstrates that BRB faults are most effectively diagnosed by analyzing the stator current spectrum under load conditions. This data is crucial for developing predictive maintenance systems that can prevent motor failure by identifying rotor bar fractures early.
e. The intelligent scheme: the validated digital twin can then be run in simulation to see how specific faults (like broken bars of varying severity) alter the motor's electromagnetic response, including its SSFR signature. This creates a known baseline and a library of fault signatures. This scheme is fundamentally different from the online, signal-based methods like MCSA. The SSFR method provides a quantitative and highly reliable means of detecting BRBs by directly measuring the resulting increases in rotor resistance (Rr) and leakage inductance (Lr). The key indicators are:

– A significant rise in the calculated Rr value (e.g., +15%).
– Asymmetry in the derived parameters when measured from different phases.
– A measurable shift and increase in the low-frequency stator impedance magnitude.

4. CONCLUSION

Establishing an easy framework of the BRB in IM is the aim of this work. The experimental test measurements of a 7.5 kW IM at standstill became the foundation for this model. The SSFR approach is an attractive method that produces accurate BRB models, is used to calculate the EC parameters. It is crucial to remember that because of BRB, the EC's resistance, self-inductance, and mutual inductance fluctuate based on how severe the fault is. The identified BRB models can be easily simulated, and their performance is validated through comparisons with results obtained using FEM. These results demonstrate that the proposed combination of SSFR and FEM modeling offers a powerful framework for the accurate modeling and diagnosis of BRB in IMs. The SSFR test provides quick and non-invasive parameter extraction, while FEM supplies detailed spatial insights into electromagnetic behavior. This synergy enhances both diagnostic accuracy and model reliability, making it suitable for integration into condition monitoring systems. Results demonstrate improved detection sensitivity and physical interpretability versus either approach used alone. This work provides practical solutions to industry challenges, benefiting both the academic working towards diagnostic and electric drive control. Additionally, future research could evaluate the potential of the proposed combination on other faults types, (eccentricity, stator winding). In addition to determining the automated fault classification for IM faults, this method should eventually integrate both ML technique.

ACKNOWLEDGMENTS

We extend our sincere thanks to everyone who contributed to the completion of this work.

FUNDING INFORMATION

Authors state no funding involved

AUTHOR CONTRIBUTIONS STATEMENT

This journal uses the Contributor Roles Taxonomy (CRediT) to recognize individual author contributions, reduce authorship disputes, and facilitate collaboration.

Name of Author	C	M	So	Va	Fo	I	R	D	O	E	Vi	Su	P	Fu
Abdelhakim Mabrek	✓	✓	✓	✓	✓	✓	✓	✓	✓	✓	✓	✓		✓
Zaidi Elyazid		✓		✓		✓	✓		✓		✓		✓	
Bachir Selmoune	✓		✓			✓	✓			✓	✓			
Kamel Eddine Hemsas		✓		✓	✓			✓	✓		✓		✓	

C : **C**onceptualization
M : **M**ethodology
So : **So**ftware
Va : **Va**lidation
Fo : **Fo**rmal analysis
I : **I**nvestigation
R : **R**esources
D : **D**ata Curation
O : Writing - **O**riginal Draft
E : Writing - Review & **E**diting
Vi : **Vi**sualization
Su : **Su**pervision
P : **P**roject administration
Fu : **Fu**nding acquisition

CONFLICT OF INTEREST STATEMENT

Authors state no conflict of interest.

INFORMED CONSENT

We have obtained informed consent from all individuals included in this study.

ETHICAL APPROVAL

The research related to human use has been complied with all the relevant national regulations and institutional policies in accordance with the tenets of the Helsinki Declaration and has been approved by the authors' institutional review board or equivalent committee.

DATA AVAILABILITY

Data availability is not applicable to this paper as no new data were created or analyzed in this study.

REFERENCES

[1] S. B. Lee *et al.*, "Condition Monitoring of Industrial Electric Machines: State of the Art and Future Challenges," *IEEE Industrial Electronics Magazine*, vol. 14, no. 4, pp. 158–167, Dec. 2020, doi: 10.1109/MIE.2020.3016138.

[2] A. K. Samanta, A. Naha, A. Routray, and A. K. Deb, "Fast and accurate spectral estimation for online detection of partial broken bar in induction motors," *Mechanical Systems and Signal Processing*, vol. 98, pp. 63–77, Jan. 2018, doi: 10.1016/j.ymssp.2017.04.035.

[3] M. Chen, Z. Zhou, B. Zhang, G. Hu, and Y. Cao, "A novel combination belief rule base model for mechanical equipment fault diagnosis," *Chinese Journal of Aeronautics*, vol. 35, no. 5, pp. 158–178, May 2022, doi: 10.1016/j.cja.2021.08.037.

[4] M. O. Mustafa, D. Varagnolo, G. Nikolakopoulos, and T. Gustafsson, "Detecting broken rotor bars in induction motors with model-based support vector classifiers," *Control Engineering Practice*, vol. 52, pp. 15–23, Jul. 2016, doi: 10.1016/j.conengprac.2016.03.019.

[5] M. Ojaghi, M. Sabouri, and J. Faiz, "Performance analysis of squirrel-cage induction motors under broken rotor bar and stator inter-turn fault conditions using analytical modeling," *IEEE Transactions on Magnetics*, vol. 54, no. 11, pp. 1–5, Nov. 2018, doi: 10.1109/TMAG.2018.2842240.

[6] H. N. Koti, H. Chen, Y. Sun, and N. A. O. Demerdash, "On shortening the numerical transient in time-stepping finite element analysis of induction motor under broken rotor bar faults," in *2019 IEEE Energy Conversion Congress and Exposition (ECCE) 2019*, Baltimore, MD, USA, Sep. 2019, pp. 1649–1654, doi: 10.1109/ECCE.2019.8912796.

[7] S. N. Hussain and S. S. H. Zaidi, "Modeling and analysis of three phase induction motor with broken rotor bar," in *17th IEEE International Multi Topic Conference: Collaborative and Sustainable Development of Technologies, IEEE INMIC 2014 - Proceedings*, Dec. 2014, pp. 488–493, doi: 10.1109/INMIC.2014.7097389.

[8] M. Skowron, "Transfer Learning-Based Fault Detection System of Permanent Magnet Synchronous Motors," *IEEE Access*, vol. 12, pp. 135372–135389, 2024, doi: 10.1109/ACCESS.2024.3463970.

[9] H. Bouzida, O. Touhami, R. Ibtiouen, M. Fadel, M. Benhaddadi, and G. Olivier, "Model structures used in rotor defect identification of a squirrel cage induction machine," *Canadian Conference on Electrical and Computer Engineering*, Ottawa, Canada, 2006, pp. 1671-1676, doi: 10.1109/CCECE.2006.277721.

[10] P. Naderi, "Cage-rotor induction motor inter-turn short circuit fault detection with and without saturation effect by MEC model," *ISA Transactions*, vol. 64, pp. 216–230, Sep. 2016, doi: 10.1016/j.isatra.2016.05.014.

[11] J. Faiz and B. M. Ebrahimi, "Locating rotor broken bars in induction motors using finite element method," *Energy Conversion and Management*, vol. 50, no. 1, pp. 125–131, Jan. 2009, doi: 10.1016/j.enconman.2008.08.025

[12] C. Wenjie *et al.*, "Time-step constraints in coupled hydro-mechanical finite element analysis of unsaturated soils," *Computers and Geotechnics*, vol. 165, 2024, doi: 10.1016/j.compgeo.2023.105914.

[13] L. Ralikalakala and M. Mojela, "Standstill Impedance Variation Test For Inverter-fed Induction Motor with Broken Rotor Bar Fault," in *International Conference on Artificial Intelligence, Computer, Data Sciences, and Applications (ACDSA) 2024* Victoria, Seychelles, Feb. 2024, pp. 1–6, doi: 10.1109/ACDSA59508.2024.1046804.

[14] B. Kim, K. Lee, J. Yang, S. B. Lee, E. J. Wiedenbrug, and M. R. Shah, "Automated detection of rotor faults for inverter-fed induction machines under standstill conditions," *IEEE Transactions on Industry Applications*, vol. 47, no. 1, pp. 55–64, Jan. 2011, doi: 10.1109/TIA.2010.2090931.

[15] C. Kral, F. Pirker, and G. Pascoli, "Detection of rotor faults in squirrel cage induction machines at standstill for batch tests by means of the Vienna monitoring method," in *Conference Record of the 2000 IEEE Industry Applications Conference. Thirty-Fifth IAS Annual Meeting and World Conference on Industrial Applications of Electrical Energy (Cat. No.00CH37129)*, Rome, Italy, 2002, pp. 499–504, doi: 10.1109/ias.2000.881156.

[16] C. Demian, A. M-Mabwe, H. Henao, and G. A. Capolino, "Detection of induction machines rotor faults at standstill using signals injection," *IEEE Transactions on Industry Applications*, vol. 40, no. 6, pp. 1550–1559, Nov. 2004, doi: 10.1109/TIA.2004.836170.

[17] M. Tahkola, Á. Szücs, J. Halme, A. Zeb, and J. Keränen, "A Novel Machine Learning-Based Approach for Induction Machine Fault Classifier Development—A Broken Rotor Bar Case Study," *Energies*, vol. 15, no. 9, pp. 1-23, May 2022, doi: 10.3390/en15093317.

[18] W. A. Elhaija and Q. A. Al-Haija, "A novel dataset and lightweight detection system for broken bars induction motors using optimizable neural networks," *Intelligent Systems with Applications*, vol. 17, pp. 1-15, Feb. 2023, doi: 10.1016/j.iswa.2022.200167.

[19] IEEE Std115, "IEEE Guide: Test Procedures for Synchronous Machines Part I– Acceptance and Performance Testing Part II-Test Procedures and Parameter Determination for Dynamic Analysis," *IEEE Std 115*. IEEE, Piscataway, NJ, USA, pp. 1–0, Nov. 07, 2010, doi: 10.1109/IEEESTD.2020.9050934.

[20] M. Abdelhakim, H. K. Eddine, E. Zaidi, and B. Selmoune, "Induction Motor Diagnosis at Standstill Conditions," in *2024 3rd International Conference on Advanced Electrical Engineering (ICAEE)*, Sidi-Bel-Abbes, Algeria, Nov. 2024, pp. 1–5, doi: 10.1109/ICAEE61760.2024.10783186.

[21] R. Nicolas, I. Marcel, D. Demba, and P. J. Chrzan, "Modeling and experimental study of 3-phase short-circuits of a double-cage induction machine," *Electric Machines and Power Systems*, vol. 27, no. 4, pp. 343–362, Mar. 1999, doi: 10.1080/073135699269190.

[22] B. Asad, T. Vaimann, A. Belahcen, A. Kallaste, A. Rassõlkin, and M. N. Iqbal, "The cluster computation-based hybrid fem–analytical model of induction motor for fault diagnostics," *Applied Sciences (Switzerland)*, vol. 10, no. 21, pp. 1–15, Oct. 2020, doi: 10.3390/app10217572.

[23] M. Bouheraoua, M. Atig, A. Bousbaine, and N. Benamrouche, "Electro-Thermal Coupled Modeling of Induction Motor Using 2D Finite Element Method," *Advances in Electrical and Computer Engineering*, vol. 21, no. 2, pp. 33–40, 2021, doi: 10.4316/AECE.2021.02004.

[24] J. Faiz and B. M. Ebrahimi, "A new pattern for detecting broken rotor bars in induction motors during start-up," *IEEE Transactions on Magnetics*, vol. 44, no. 12, pp. 4673–4683, Dec. 2008, doi: 10.1109/TMAG.2008.2002903.

[25] M. C. H. Nguyen and C. D. Tran, "An extended sensor fault tolerant control method applied to three-phase induction motor drives," *Bulletin of Electrical Engineering and Informatics*, vol. 13, no. 1, pp. 125–133, Feb. 2024, doi: 10.11591/eei.v13i1.5992.
[26] A. Mabrek and K. E. Hemsas, "Induction motor inter-turn fault modeling and simulation using SSFR test for diagnosis purpose," *Automatika*, vol. 57, no. 4, pp. 948–959, Oct. 2016, doi: 10.7305/automatika.2017.10.1805.
[27] S. Tabet, A. Ghoggal, H. Razik, I. Amrani, and S. E. Zouzou, "Experimental and simulation investigation for rotor bar fault diagnosis in closed-loop induction motors drives," *Bulletin of Electrical Engineering and Informatics*, vol. 12, no. 4, pp. 2058–2068, Aug. 2023, doi: 10.11591/eei.v12i4.4833.

BIOGRAPHIES OF AUTHORS

Abdelhakim Mabrek received the engineer from the University of M'sila, Algeria in 2006, he received Magister and Doctorate from the University of Setif 1 Algeria in 2011, 2018. Currently he is Research Professor in Electromechanical Institution, EL Bachir El Ibrahimi University, Bordj Bou Arreridj, Algeria. Member in intelligent materials and renewable energy laboratory (LMIER), his main fields of interest are the induction motor drive control and state variable estimation, and its application for diagnostic problems of AC electrical drives. He can be contacted at email: abdelhakim.mabrek_1@univ-bba.dz.

Zaidi Elyazid was born in Bordj Bou Arreridj, Algeria. He received his master's degree in 2017 and his doctorate in 2022 from the University of Mohamed El Bachir El Ibrahimi in Bordj Bou Arreridj, Algeria. He is employed as a full professor in Electrical Engineering Department of Bordj Bouarreridj University. His main fields of interest are control techniques neuro-fuzzy logic control, MATLAB simulation, mechatronics, automation and robotics and advanced control theory. He can be contacted at email: elyazid.zaidi@univ-bba.dz.

Bachir Selmoune was born in Bordj Bou Arreridj, Algeria, in 1994. He obtained his master's degree in 2018 and his doctorate in 2023 from the University of Mohamed El Bachir El Ibrahimi in Bordj Bou Arreridj, Algeria. He is affiliated with the LPMRN Laboratory at the University of Mohamed El Bachir El Ibrahimi in Bordj Bou Arreridj, 34000 Algeria. His primary focus areas include modeling electromagnetism and electrical control, as well as their practical applications. He can be contacted at email: bachir34selmoune@gmail.com.

Kamel Eddine Hemsas was born in Setif, Algeria. He received the engineer, Magister and Doctorate from the University of Setif 1 Algeria in 1991, 1995, and 2005, respectively. He is a full professor in Electrical Engineering Department, and head of research at the same university. His areas of interest include on power quality issues, modeling, control diagnosis and state observer of electric machine and systems, renewable energy and artificial intelligence. He is the author of several international publications, communications and two books. He can be contacted at email: hemsas_ke_dz@univ-setif.dz.